Novel Broadband Monopole Antennas With Dual-Band Circular Polarization

Christina F. Jou, Jin-Wei Wu, and Chien-Jen Wang, *Senior Member, IEEE*

Abstract—Novel broadband monopole antenna designs with dual-band circular polarization (CP) are presented. The proposed antenna comprised of a ground plane embedded with an inverted-L slit, which is capable of generating a resonant mode for broadband impedance-bandwidth, and excites two orthogonal E vectors with equal amplitude and 90 ° phase difference (PD) for radiating left-hand circular polarization (LHCP) at 2.5 GHz and right-hand circular polarization (RHCP) at 3.4 GHz. A bevel is cut in the rectangular radiator to increase the impedance-bandwidth. The measured result of the impedance-bandwidth is about 4.46 GHz from 2.12 to 6.58 GHz; the 3-dB axial ratio (AR) bandwidths are about 150 MHz at the lower band (2.5 GHz) and 230 MHz at the upper band (3.4 GHz). Furthermore, embedding an I-shaped slit in the rectangular radiator and adding an I-shaped stub in the ground plane, the impedance-bandwidth can be further increased to 6.30 GHz (2.17–8.47 GHz), and the 3-dB AR-bandwidth at the upper band is greatly enhanced from 230 to 900 MHz.

Index Terms—Axial ratio (AR), broadband antennas, circular polarization (CP), monopole antennas.

I. INTRODUCTION

IN recent years, printed monopole antennas have been developed since they have many attractive features such as simple structure, low profile, light weight, wide impedance-bandwidth, and omnidirectional radiation patterns [1]–[3]. The antennas are widely used for the wireless communication systems such as GSM, DCS, PCS, IMT-2000, WLAN, and UWB. However, these printed antennas are both tall and wide; they are few applications in handheld devices. In general, the radiation patterns of the printed monopole antennas are linearly polarized (LP); they are difficult to radiate circularly polarized (CP) radiation wave which was generated by two near-degenerated orthogonal resonant modes of equal amplitude and 90 ° phase difference (PD). The essential feature of polarization diversity is that the signal reception performance can be improved in the multipath fading environment [4]. Therefore, the circularly polarized antennas are often utilized in radar, satellite, radio frequency identification (RFID), navigation, and sensor systems. If the monopole antenna can generate the LP and CP radiation waves, the applications of the monopole antenna will be greatly enhanced.

C. F. Jou and J.-W. Wu are with the Department of Communication Engineering, National Chiao-Tung University, Hsinchu, Taiwan, R.O.C.

C.-J. Wang is with the Department of Electronics Engineering, National University of Tainan, Tainan, Taiwan, R.O.C. (e-mail: cjwang@mail.nutn.edu.tw).

Color versions of one or more of the figures in this paper are available online at http://ieeexplore.ieee.org.
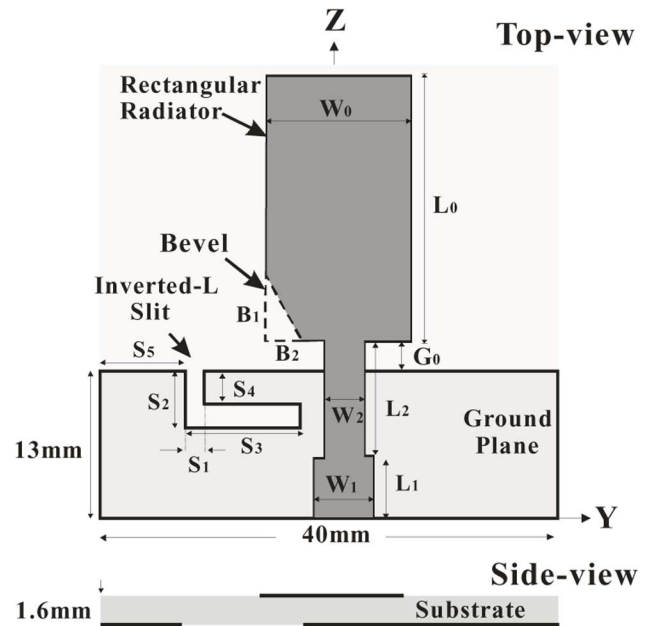
Fig. 1. Antenna 1, configurations of the proposed printed monopole antenna with inverted-L slit.

Typically, the planar CP antenna is achieved through using patch antenna [5]–[8] and slot antenna [9]–[12]. Previous reports in [5] and [6] show that a CP patch antenna is introduced by cutting slot. A coupling method of a fan-shaped patch for CP antenna has been investigated in [7]. To reduce the size of CP antenna, a cross-patch with a dual-band hybrid is proposed [8]. These antennas can excite a pure CP radiation wave, but the impedance- and AR-bandwidth are narrower than 10%. To generate wider AR-bandwidth, many printed slot antennas are designed [9]–[12]. In [9] and [10], the antenna structures contain a ring slot which produces CP radiation waves by embedding a slot or adding a shorted strip. In addition to ring slot, a crosspatch-loaded is added in the centre of the square slot [11] and a mono-strip is added in the circular slot [12] to excite two near-degenerate orthogonal resonant modes of equal amplitude and 90 ° phase difference for CP. In fact, the 3-dB AR-bandwidth of slot antennas can be larger than 10%. However, the 10-dB impedance-bandwidth is less than 50%.

In this paper, novel broadband monopole antennas with dual-band CP are proposed. A microstrip-fed monopole antenna with an inverted-L slit in the ground plane, called Antenna 1, is presented in Fig. 1. It gives a broadband impedance-bandwidth of 102.5% at the center frequency of 4.35 GHz and the dual-band CP radiation waves of 6.0% LHCP at the center frequency of 2.485 GHz (lower band) and 6.7% RHCP at the center frequency of 3.425 GHz (upper band). In addition, Fig. 2 shows Antenna 2, which is designed by embedding an I-shaped slit in monopole
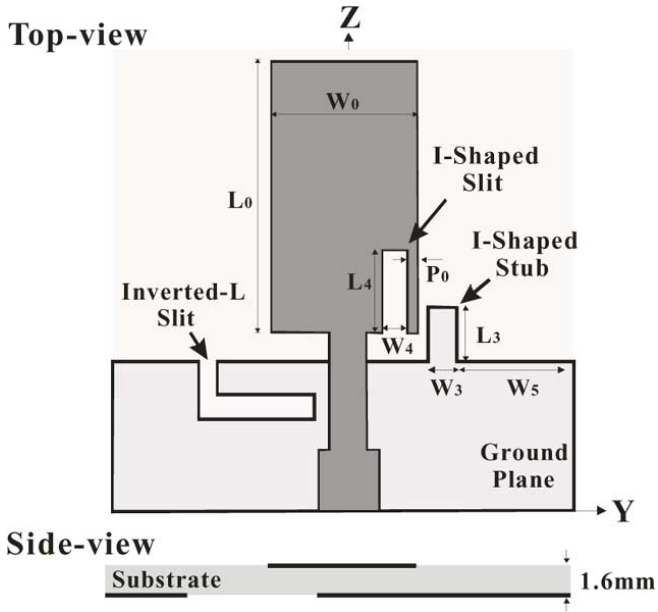
Fig. 2. Antenna 2, configurations of the proposed printed monopole antenna with inverted-L slit, I-shaped slit, and I-shaped strip.

radiator and adding an I-shaped stub in ground plane. It can further increase the impedance-bandwidth to 118.4% and enhance the 3-dB AR-bandwidth at the upper band to 23.1%. The results show that the two novel antennas can achieve broadband impedance-bandwidth and dual-band CP. The impedance- and AR-bandwidth are better than patch and slot antenna.

II. DESIGN OF ANTENNA 1 AND 2

The schematic diagrams of the proposed monopole antennas are illustrated in Figs. 1 and 2, respectively. They were etched on 1.6–mm-thick FR4 substrate with relative permittivity $\varepsilon_r = 4.4$ and loss tangent $\tan \delta = 0.024$. The overall dimensions of the antennas are about $40 \times 39 \times 1.6$ mm^3. In general, the length of monopole antenna is usually about a quarter-wavelength. The approximate value for the length L_0 of monopole radiating strip is given by

$$L_0 \approx \frac{\lambda_g}{4} = \frac{\lambda_r}{4\sqrt{\varepsilon_{\text{eff}}}} = \frac{c}{4\sqrt{\varepsilon_{\text{eff}}}f_r} \qquad (1)$$

with

$$\varepsilon_{\text{eff}} = \frac{\varepsilon_r + 1}{2} \qquad (2)$$

where c is the speed of light, λ_r is the free-space wavelength of the monopole resonant frequency f_r, and ε_{eff} is the approximated effective dielectric constant [13]. The dimensions of the rectangular radiator of the antennas $(L_0 \times W_0)$ are 23.5×12 mm^2.

A. Antenna 1 Design

The general behavior of a monopole antenna is either vertical or horizontal linearly polarized. If the conventional monopole antenna is vertically linearly polarized, the radiation in the horizontal direction is very weak. For this reason, the conventional monopole antenna is very difficult to excite CP. CP is generated by two orthogonal E vectors $(E_{\text{Hor}}, E_{\text{Ver}})$ with equal am-

plitude and 90 ° phase difference (PD), where E_{Hor} and E_{Ver} denote the complex voltage in the horizontal and vertical plane, respectively.

To achieve the CP radiation wave, see Fig. 1, an inverted-L slit is embedded in the ground plane at the left side of the feed line. The E_{Hor} of the inverted-L slit and E_{Ver} of the rectangular radiator have a phase difference of 90 ° which can excite CP. The phase of the E_{Hor} leads E_{Ver} about 90 ° and the LHCP wave at the lower frequency (2.5 GHz) can be generated. At the upper frequency (3.4 GHz), a RHCP wave is also excited, because there is a 90 ° phase lag instead of 90° phase lead as in the lower band. The effect of the length of inverted-L slit $(S_2 + S_3)$ on the AR will be discussed in Section IV.

The impedance-bandwidth can also be increased by this technique. In the operating frequency range, three resonant modes are excited by the rectangular radiator and one resonant mode is excited by the ground plane with the inverted-L slit.

Furthermore, a bevel is cut to adjust the impedance matching [14]. Also, a 50–Ohm microstrip feed line of width W_1 and length L_1 is terminated with the standard SMA connector and connected to an impedance transformer of width W_2 and length L_2.

B. Antenna 2 Design

To further enhance the impedance- and AR-bandwidth, the I-shaped slit and stub are added in the rectangular radiator and ground plane, respectively. The geometry of this Antenna 2 is shown in Fig. 2. The I-shaped slit of length L_4 in the rectangular radiator can excite a RHCP wave at the upper frequency band. The I-shaped stub of length L_3 in the ground plane can affect the phase difference. The AR-bandwidth of the upper band can be increased by adjusting the sizes of L_3 and L_4. The detail effects about the length (L_3, L_4) will be studied in Section IV. Furthermore, the I-shaped slit and stub can excite a mode at 8.0 GHz, so that the impedance-bandwidth is further extended to 6.30 GHz.

The positions of the I-shaped slit and stub can interfere with the antenna performance resulting from tuning the inverted-L slit. If the positions of the I-shaped slit and stub are designed at the left side of the feed line, the characteristics of the extremely wide impedance-bandwidth and dual-band CP will be destroyed. Therefore, they are embedded at the right side of the feed line. Detailed dimensions are listed in Table. I.

III. SIMULATION AND MEASUREMENT RESULTS

There are three subsections: A) Studying the impedance-bandwidth and resonant modes. The simulated and measured return loss of Antenna 1 and 2 are discussed. The resonant modes are explained by the simulated surface current distributions for Antenna 1 and 2. B) Analyzing axial ratios. The simulated and measured results of AR will show that Antenna 1 has dual-band CP and Antenna 2 enhances the AR-bandwidth at the upper band. C) Illustrating the measured radiation patterns and gains.

A. Impedance Bandwidth and Resonant Modes

The characteristics of the two monopole antennas were calculated by Ansoft High Frequency Structure Simulator (HFSS) software and measured by HP 8722C network analyzer.

TABLE I
DIMENSIONS OF THE PROPOSED PRINTED ANTENNA 1 AND 2

	Antenna1	Antenna2		Antenna1	Antenna2
L_0	23.5 mm	23.5 mm	W_0	12 mm	12 mm
L_1	6.0 mm	6.0 mm	W_1	3.0 mm	3.0 mm
L_2	9.5 mm	9.1 mm	W_2	2.4 mm	2.4 mm
L_3	-	3.5 mm	W_3	-	0.5 mm
L_4	-	8.2 mm	W_4	-	1.2 mm
S_1	1.0 mm	1.0 mm	W_5	-	13 mm
S_2	6.0 mm	6.0 mm	P_0	-	1.0 mm
S_3	11.0 mm	11.0 mm	B_1	5.0 mm	-
S_4	4.7 mm	4.0 mm	B_2	2.5 mm	-
S_5	7.0 mm	7.0 mm	G_0	2.5 mm	2.1 mm
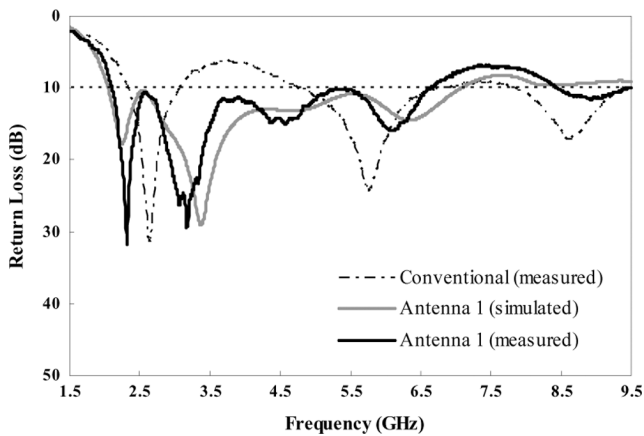
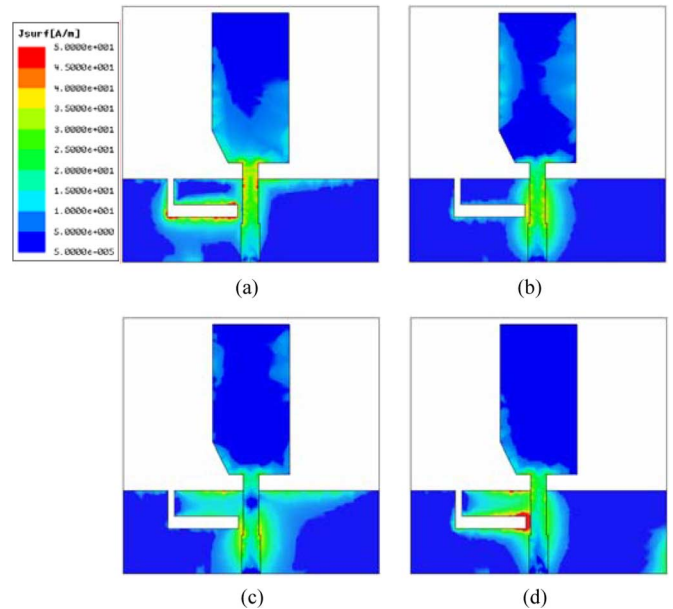Fig. 3. Simulated and measured return loss of the conventional antenna and Antenna 1.

Fig. 4. Simulated surface current distributions of Antenna 1: three resonant modes of monopole (a) 2.25 GHz; (b) 4.65 GHz; (c) 6.35 GHz; and one resonant mode of ground plane (d) 3.35 GHz.

Antenna 1: Fig. 3 compares the simulated and measured return loss for a conventional monopole antenna and Antenna 1. In our experiments, the conventional monopole antenna consists of a feed line, a rectangular radiator without the slit and bevel, and a ground plane without the slit and stub. The measured impedance-bandwidth of Antenna 1 for 10-dB return loss is from 2.12 to 6.58 GHz, which has about 4.46 GHz bandwidth (102.5%), comparing to the conventional antenna only has 0.73 GHz bandwidth (27%) from 2.34 to 3.07 GHz. According to the result of measured return loss, Antenna 1 performs a wide bandwidth due to the four resonant modes which are influenced and excited by the inverted-L slit. From the simulated result, these four resonant modes are: the three resonant modes of monopole antenna at the center frequencies of 2.25, 4.65, and 6.35 GHz, and one resonant mode of the ground plane at the center frequency of 3.35 GHz. In Fig. 4, the simulated surface current distributions are presented for these four resonant modes. In Fig. 4(a), (b), and (c), the simulation results show that the three resonant modes of monopole antenna are influenced by the inverted-L slit. Fig. 4(d) shows the most surface current distributions are formed along the inverted-L slit to excite the resonant mode of the ground plane. Therefore, the ground embedded inverted-L slit can be used to excite extra resonant mode, which provides extended bandwidth.

Fig. 5 describes the effect of the cutting bevel on the measured return loss. For the rectangular radiator without the bevel, the third and fourth resonant modes of the Antenna 1 are excited at 4.40 and 6.40 GHz, respectively. With the presence of

the cutting bevel, the third mode is shifted to higher frequency and the fourth mode is shifted to the lower frequency. Thus, the impedance-bandwidth can be increased.

Based on the discussion above, we can realize that due to the combination of the four resonant modes, the impedance-bandwidth can be increased from 27% of conventional monopole antenna to 102.5% of Antenna 1. The experimental results verify that the method of embedding inverted-L slit in ground plane and cutting the bevel in the rectangular radiator can increase impedance-bandwidth.

Antenna 2: Fig. 6 illustrates the simulated and measured return loss of Antenna 2. The 10-dB bandwidth of measured return loss is extended to 6.30 GHz or about 118.4%, covering the range from 2.17 to 8.47 GHz. The resonant modes of Antenna 2 are at: 2.93, 3.37, 6.0, and 8.0 GHz which are affected by embedding the I-shaped slit and adding I-shaped stub. Therefore, these resonant modes are differed from Antenna 1. From Fig. 7(a)–(c), it can be clearly seen that the resonances at 2.93, 3.37, and 6.0 GHz are interfered with the I-shaped slit in the rectangular radiator and the I-shaped stub in the ground plane. In addition, this method excites one resonant mode at 8.0 GHz.
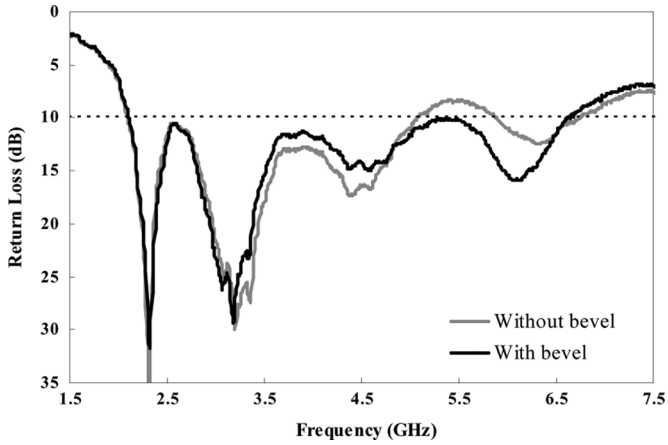
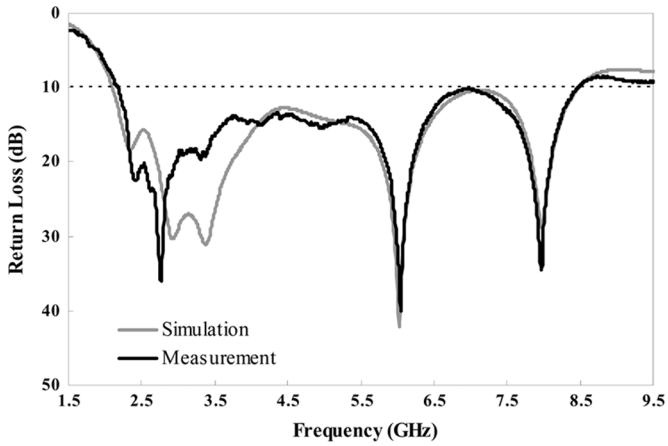Fig. 5. Comparison the measured return loss of Antenna 1 with and without the bevel.

Fig. 6. Simulated and measured return losses against frequency for the proposed Antenna 2.
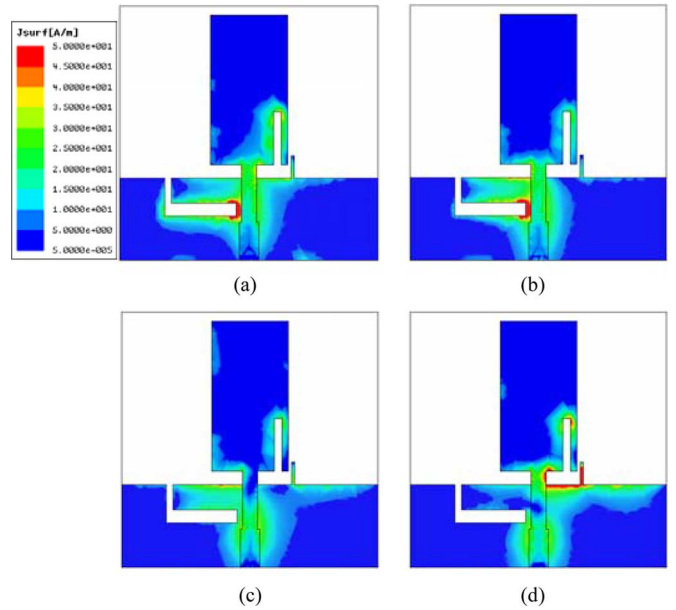

Fig. 7. Simulated surface current distributions of Antenna 2: (a) 2.93 GHz; (b) 3.37 GHz; (c) 6.00 GHz; and (d) 8.00 GHz.

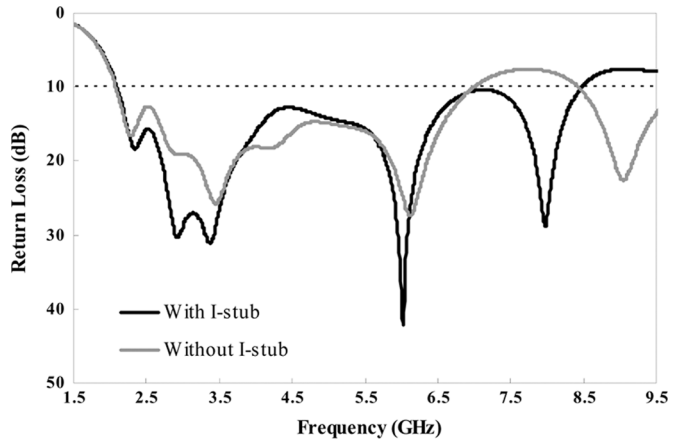Fig. 8. Comparison the simulated return loss of Antenna 2.

In Fig. 7(d), the maximum surface current is localized in the I-shaped stub and slit to yield a resonant mode at 8.0 GHz. Due to the four resonant modes affected by the I-shaped stub and slit, they combined to form a broadband impedance-bandwidth.

The simulated return loss of the Antenna 2 with and without I-shaped stub is compared in Fig. 8. A resonant mode at the center frequencies of 9.0 GHz can be shifted to 8.0 GHz by using I-shaped stub to increase the impedance-bandwidth. Furthermore, this technique of embedding the I-shaped slit and stub can also improve the AR-bandwidth at the upper band (3.4 GHz band). Details of the results of AR will be described in next subsection.

B. Axial Ratios

Antenna 1: The simulated and measured AR and PD results of the lower and upper bands at the broadside direction are plotted in Fig. 9(a) and (b). The measured 3-dB AR-bandwidths reach 150 MHz from 2.41 to 2.56 GHz (lower band) or about 6.0% with respect to the center frequency at 2.485 GHz, and 230 MHz from 3.31 to 3.54 GHz (upper band) or about 6.7% with respect to the center frequency at 3.425 GHz. From the measured PD results, the PD of the lower band is close to 90 ° to generate a LHCP wave, and a RHCP wave is achieved at the upper band by the PD of $-90°$. In addition, the measured PD

as function of frequency varies less than the simulation result; therefore the measured 3-dB AR-bandwidth is wider than the simulation. From the results, we can see that the AR-bandwidth could be greatly increased, if the variation of the PD can be kept about 90 ° or -90 ° as function of frequency.

Antenna 2: Fig. 10(a) and (b) shows the simulated and measured AR and PD results of the lower and upper bands at the broadside direction. From Fig. 10(a), it appears that the 3-dB AR-bandwidth is from 2.41 to 2.55 GHz approximately 5.6% with respect to the center frequency at 2.48 GHz. To compare Fig. 9(a) to Fig. 10(a), it can be found that the characteristic of AR at the lower band is slightly affected by the I-shaped slit and stub.

From the measured results of upper band which compare Fig. 10(b) with Fig. 9(b), we can see the first CP mode (3.6 GHz) excited by inverted-L slit and the second CP mode (4.2 GHz) generated by the I-shaped slit and stub are combined to form a wider AR-bandwidth at the upper band than Antenna 1. In addition, the variation of the PD at the upper band can
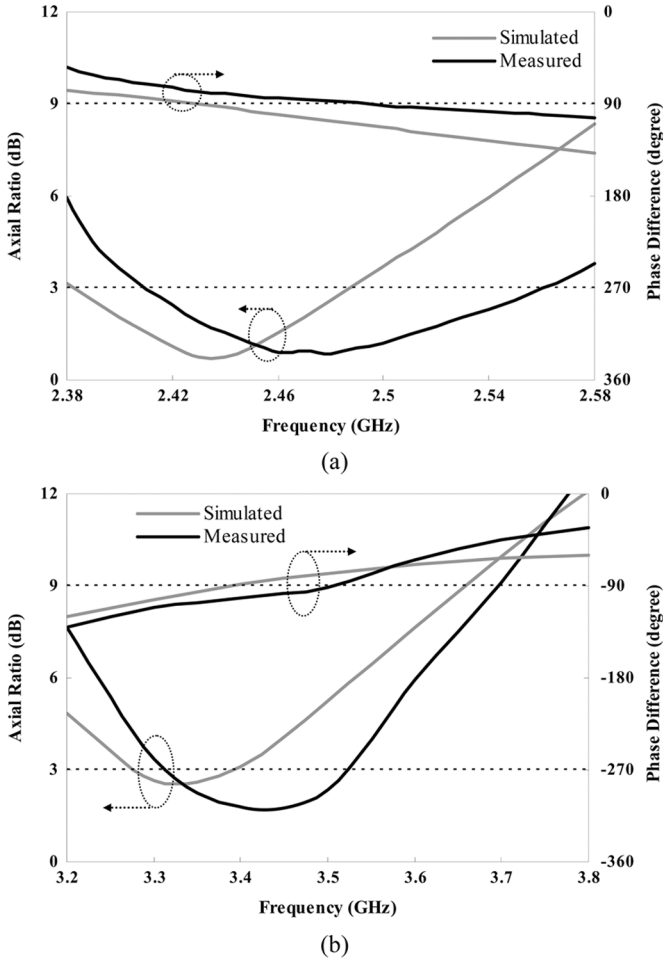
Fig. 9. Simulated and measured axial ratio and phase difference of Antenna 1. (a) Lower band. (b) Upper band.

Fig. 10. Simulated and measured axial ratio and phase difference of Antenna 2. (a) Lower band. (b) Upper band.

be kept about $-90°$ from 3.5 to 4.2 GHz by the I-shaped slit and stub. The measured 3-dB AR-bandwidth can greatly extend to about 900 MHz from 3.45 to 4.35 GHz or about 23.1% with respect to the center frequency at 3.90 GHz. Thus, the AR-bandwidth of Antenna 2 at the upper band has been improved from 6.7% of Antenna 1 to 23.1% of Antenna 2. The measured minimum AR of LHCP is 0.41dB at 2.49 GHz and RHCP is 0.71 dB at 4.2 GHz.

The performances of the conventional and two proposed Antennas are summarized in Table II. In Antenna 1, inverted-L slit can greatly increase impedance-bandwidth and excite dual-band CP. In Antenna 2, the impedance- and AR-bandwidth at the upper band can be further improved by embedding an I-shaped slit and adding an I-shaped stub.

C. Radiation Patterns and Gains

The measured normalized radiation patterns at XY-plane and XZ-plane of Antenna 1 are displayed in Fig. 11. It is noted that the radiation patterns are not omnidirectional because the structure of the proposed antennas is not symmetrical and the radiation patterns are influenced by slit and stub. Therefore, it can not achieve the requirement for handheld devices. We observe that good LHCP and RHCP radiation patterns are excited in the lower and upper band, respectively. The measured 3-dB AR beam widths in the XY- and XZ-plane are 101° and 34°,
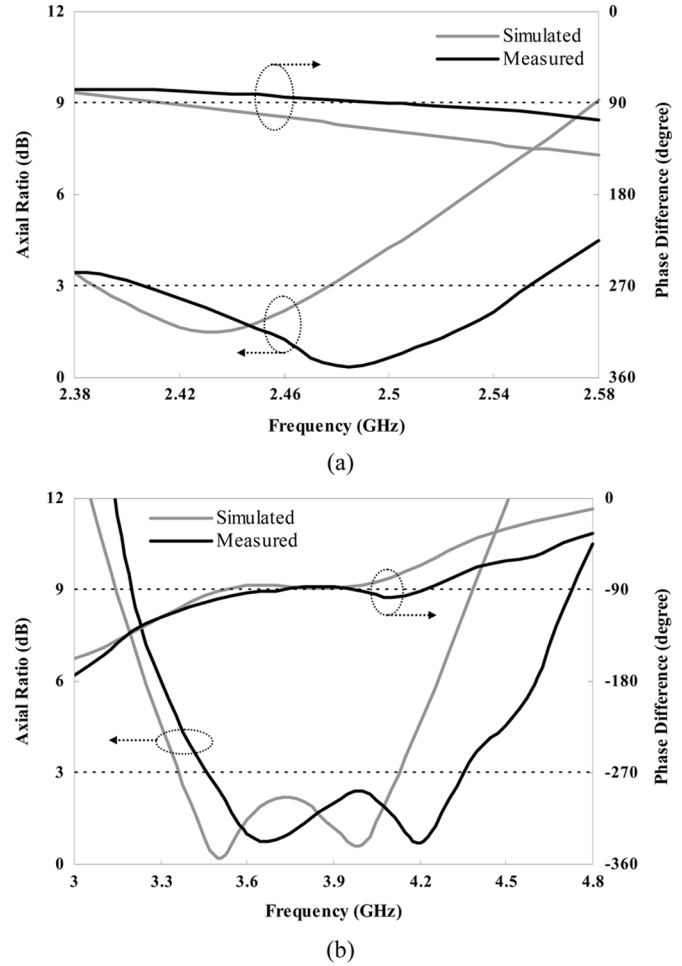
respectively, at 2.50 GHz in Fig. 11(a). In Fig. 11(b), the 3-dB AR beam widths are 49° and 24° at 3.44 GHz. The measured normalized radiation patterns of Antenna 2 at three different frequencies of 2.49, 3.70, and 4.20 GHz are shown in Fig. 12. The measured 3-dB AR beamwidths of Antenna 2 at 2.49, 3.70, and 4.20 GHz are 88°, 76°, and 66°, respectively, in the XY-plane. In the XZ-plane are 27°, 31°, and 27°. In addition, the maximum measured gains of Antenna 2 at 2.40, 3.70, and 4.20 GHz are about 0.77, 0.97, and 1.92 dBi, respectively. From Figs. 11 and 12, the CP of the antenna at $+X$ and $-X$ direction is the opposite polarization, the reason is because the E_{Ver} on the top and bottom surface of the substrate remains the same phase; however, the E_{Hor} on the top and bottom surface of the substrate is 180° out of phase.

IV. PARAMETRIC STUDIES

This section focuses on the effects of various parameters on the AR. The performance of AR at the broadside direction is mainly affected by the dimensions of inverted-L slit $(S_2 + S_3)$ of Antenna 1, and I-shaped slit (L_4) and I-shaped stub (L_3) of Antenna 2.

A. Inverted-L Slit of Antenna 1

Fig. 13 exhibits the effects of adjusting the total length of inverted-L slit $(S_2 + S_3)$ of Antenna 1 on the center frequency

TABLE II
PERFORMANCE OF CONVENTIONAL AND PROPOSED ANTENNAS

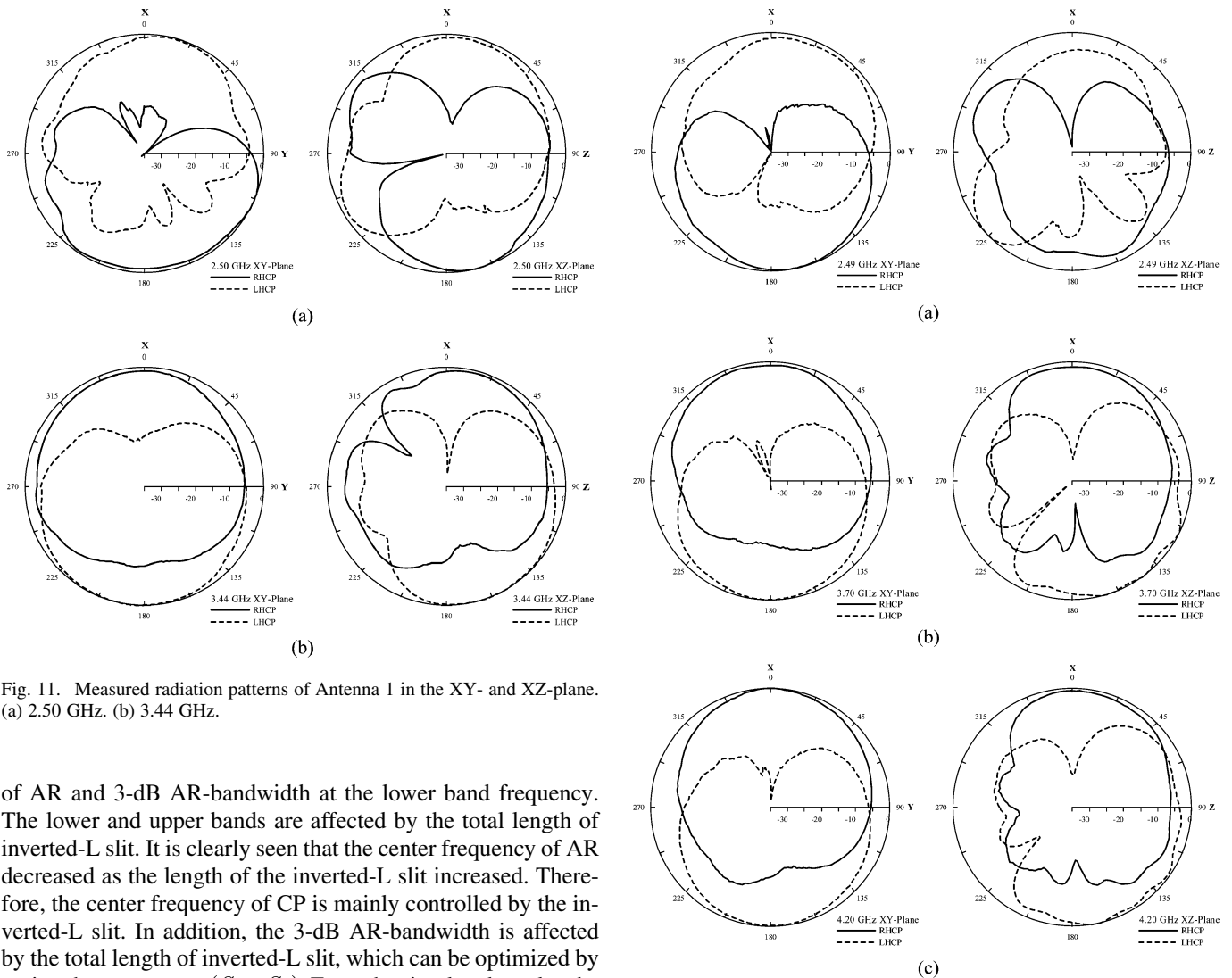|	Conventional	Antenna 1	Antenna 2
f_{lowest} (GHz)	2.34	2.12	2.17
Imp. BW (GHz, %)	0.73, 27 %	4.46, 102.5 %	6.30, 118.4 %
Lower-band AR-BW (MHz, %)	none	150, 6.0 %	140, 5.6 %
Upper-band AR-BW (MHz, %)	none	230, 6.7 %	900, 23.1 %
Polarization	LP	CP : 2.41 ~ 2.56 GHz 3.31 ~ 3.54 GHz LP : others	CP : 2.41 ~ 2.55 GHz 3.45 ~ 4.35 GHz LP : others

Fig. 11. Measured radiation patterns of Antenna 1 in the XY- and XZ-plane. (a) 2.50 GHz. (b) 3.44 GHz.

of AR and 3-dB AR-bandwidth at the lower band frequency. The lower and upper bands are affected by the total length of inverted-L slit. It is clearly seen that the center frequency of AR decreased as the length of the inverted-L slit increased. Therefore, the center frequency of CP is mainly controlled by the inverted-L slit. In addition, the 3-dB AR-bandwidth is affected by the total length of inverted-L slit, which can be optimized by tuning the parameters $(S_2 + S_3)$. From the simulated results, the characteristic of CP is determined by the length of inverted-L slit $(S_2 + S_3)$.

B. I-Shaped Slit and Stub of Antenna 2

The simulated upper band AR and PD results of Antenna 2 at the different length of I-shaped slit (L_4) are plotted in Fig. 14. The I-shaped slit with three different lengths, 7.2, 8.2, and 9.2 mm, are analyzed as other parameters are fixed. From

Fig. 12. Measured radiation patterns of Antenna 2 in the XY- and XZ-plane. (a) 2.49 GHz. (b) 3.70 GHz. (c) 4.20 GHz.

Fig. 14(a), the first CP mode is about 3.5 GHz, which is excited by inverted-L slit, and it is affected slightly when varying the length L_4. However, the second CP mode is strongly dependent on L_4. When $L_4 = 9.2$ mm, there is only one CP mode. Thus, the 3-dB AR-bandwidth is quite narrow. From the case of $L_4 = $
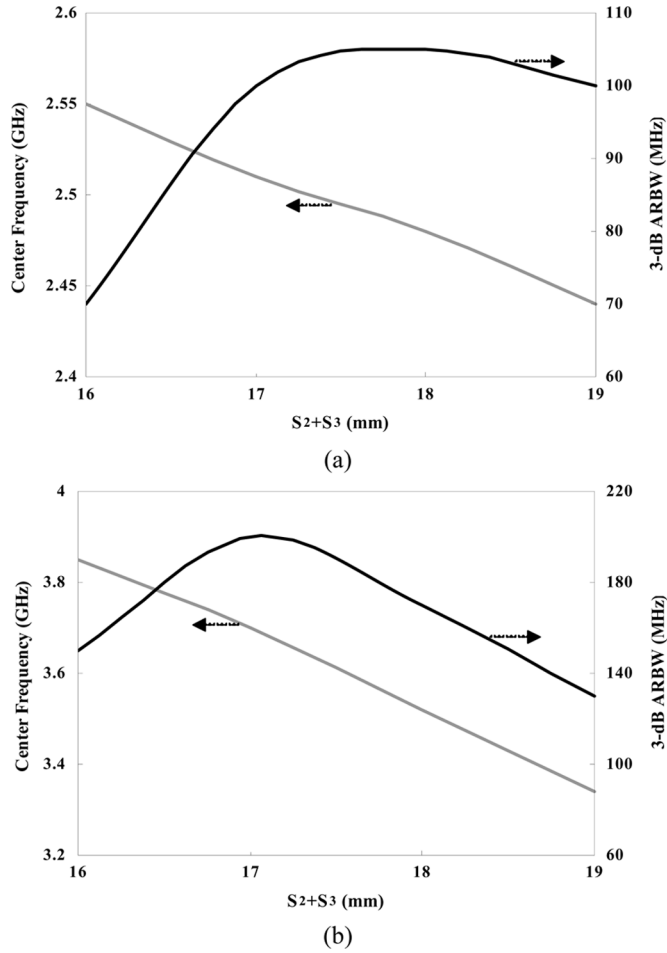
Fig. 13. Simulated center frequency of axial ratio and 3-dB axial ratio bandwidth for the inverted-L length of Antenna 1. (a) Lower band. (b) Upper band.
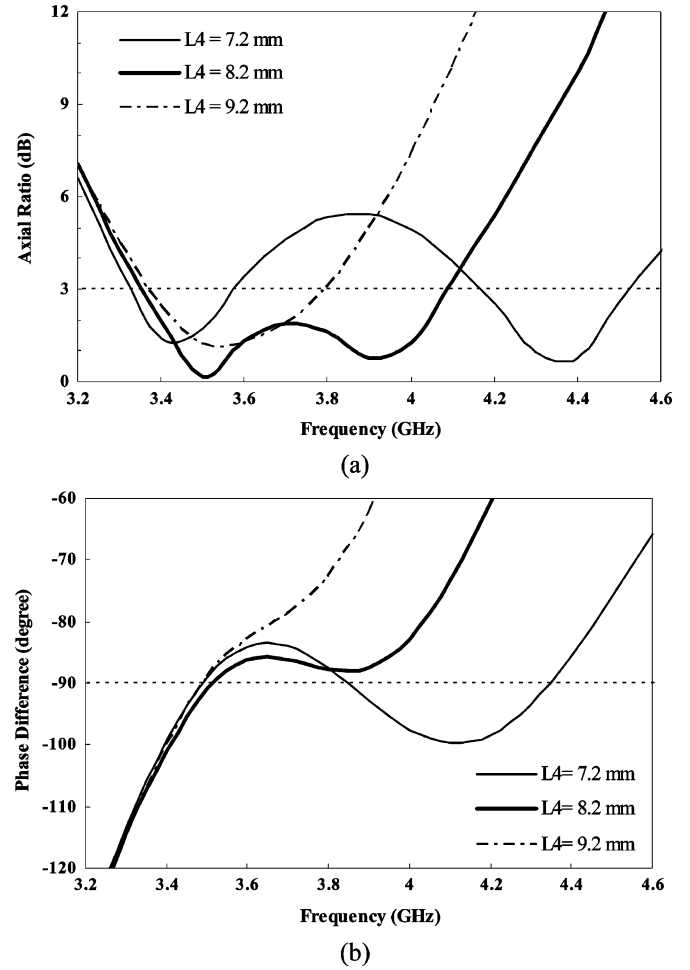

Fig. 14. Simulated phase difference and axial ratio of the I-shape slit length of Antenna 2 at upper band. (a) Axial ratio. (b) Phase difference.

8.2 mm, two CP modes are shown and the two bands resulting from the two CP modes are merged into one broad CP band. As L_4 is decreased to 7.2 mm, the frequency of the second CP mode is increased to 4.36 GHz, so that the upper band is turned into two bands. Therefore, by properly tuning L_4, the two CP modes can be combined to form a wider AR-bandwidth. However, from Fig. 14(b), it can clearly be found that although for $L_4 = 7.2$ mm, the PD is kept roughly $-90°$ at 3.8 GHz, but the AR [see Fig. 14(a)] is not less than 3 dB at 3.8 GHz. Therefore, because the magnitudes of two orthogonal E vectors are not equal, this radiation wave becomes elliptic polarization instead of circular polarization at 3.8 GHz. Based on this study, we choose $L_4 = 8.2$ mm.

The effects of the length of I-shaped stub L_3 on AR and PD at the upper band are depicted in Fig. 15. From studying these data, there are two important points to be found. First, in Fig. 15(a), the length of I-shaped stub can affect the second CP mode of the upper band. However, compared with Fig. 14(a), L_4 is more affective than L_3 for tuning the second CP mode. Second, from Fig. 15(b), it is observed that the variation of PD can be tuned by different L_3. Note that the variation of PD is important for CP. When $L_3 = 4.0$ mm, the variation of PD from 3.5 to 3.9 GHz is kept roughly $-90°$ in Fig. 15(b), and the AR is also less than 1.5 dB to activate a good CP in Fig. 15(a).

According to these study results of L_4 and L_3, the frequency of the second CP mode is mainly controlled by L_4, and the PD of the second CP mode is mainly controlled by L_3. Therefore, the widest 3-dB AR-bandwidth can be reached at the upper band by properly adjusting L_4 and L_3.

V. CONCLUSION

The broadband monopole antennas with dual-band circular polarization have been developed. In Antenna 1 design, an inverted-L slit embedded in the ground plane can not only be used to enhance the impedance-bandwidth, but also to excite dual-band circularly polarized radiation waves. The measured impedance-bandwidth is 102.5% from 2.12 to 6.58 GHz, and the 3-dB AR-bandwidths of dual-band CP wave are about 6.0% for LHCP at the lower band and 6.7% for RHCP at the upper band. Furthermore, a method used to enhance the impedance- and AR-bandwidth is proposed. Antenna 2 demonstrates by embedding an I-shaped slit in the rectangular radiator and by adding an I-shaped stub in the ground plane can further increase the impedance-bandwidth and AR-bandwidth of the upper band. The measured results show that the impedance-bandwidth was enhanced from 102.5% to 118.4%, and the 3-dB AR-bandwidth
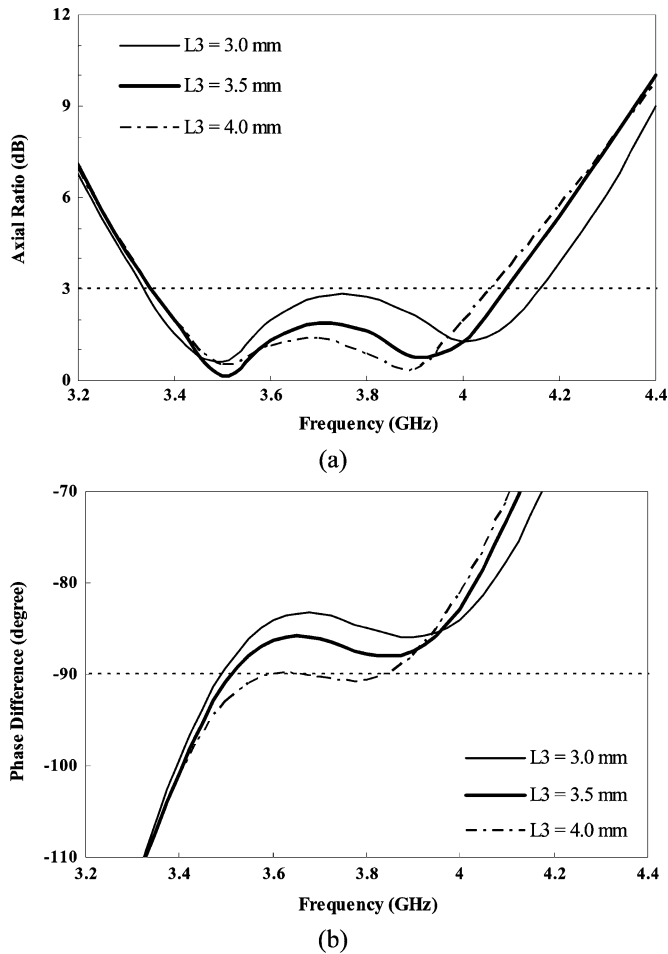
Fig. 15. Simulated phase difference and axial ratio of the I-shape stub length of Antenna 2 at upper band. (a) Axial ratio. (b) Phase difference.

at the upper band was improved from 6.7% to 23.1%. The proposed antennas, which have simple structure, excellent performances, and fabricated easily, are very suitable for the modern wireless commutation system.

REFERENCES

[1] J. Liang, C. C. Chiau, X. Chen, and C. G. Parini, "Printed circular disc monopole antenna for ultra-wideband applications," *Electron. Lett.*, vol. 40, no. 20, pp. 1246–1247, Sep. 2004.

[2] Z. N. Chen, M. J. Ammann, M. Y. W. Chia, and T. S. P. See, "Annular planar monopole antennas," *Inst. Elect. Eng. Proc.-Microw. Antennas Propag.*, vol. 149, no. 4, pp. 200–203, Aug. 2002.

[3] C. C. Lin, Y. C. Kan, L. C. Kuo, and H. R. Chuang, "A planar triangular monopole antenna for UWB communication," *IEEE Microw. Wireless Compon. Lett.*, vol. 15, no. 10, pp. 624–626, Oct. 2005.

[4] S. H. Hsu and K. Chang, "A novel reconfigurable microstrip antenna with switchable circular polarization," *IEEE Antennas Wireless Propag. Lett.*, vol. 6, pp. 160–162, 2007.

[5] S. M. Kim, K. S. Yoon, and W. G. Yang, "Dual-band circular polarization square patch antenna for GPS and DMB," *Microw. Opt. Technol. Lett.*, vol. 49, no. 12, pp. 2925–2926, Dec. 2007.

[6] K. F. Tong and T. P. Wong, "Circularly polarized U-slot antenna," *IEEE Trans. Antennas Propag.*, vol. 55, no. 8, pp. 2382–2385, Aug. 2007.

[7] Y. F. Lin, H. M. Chen, and S. C. Li, "A new coupling mechanism for circularly polarized annular-ring patch antenna," *IEEE Trans. Antennas Propag.*, vol. 56, no. 1, pp. 11–16, Jan. 2008.

[8] H. Y. A. Yim, C. P. Kong, and K. K. M. Cheng, "Compact circularly polarised microstrip antenna design for dual-band applications," *Electron. Lett.*, vol. 42, no. 7, pp. 380–381, Mar. 2006.

[9] J. Y. Sze, C. I. G. Hsu, M. H. Ho, Y. H. Ou, and M. T. Wu, "Design of circularly polarized annular-ring slot antennas fed by a double-bent microstripline," *IEEE Trans. Antennas Propag.*, vol. 55, no. 11, pp. 3134–3139, Nov. 2007.

[10] K. M. Chang, R. J. Lin, I. C. Deng, and Q. X. Ke, "A novel design of a microstrip-fed shorted square-ring slot antenna for circular polarization," *Microw. Opt. Technol. Lett.*, vol. 49, no. 7, pp. 1684–1687, Jul. 2007.

[11] C. C. Chou, K. H. Lin, and H. L. Su, "Broadband circularly polarised crosspatch-loaded square slot antenna," *Electron. Lett.*, vol. 43, no. 9, pp. 485–486, Apr. 2007.

[12] I. C. Deng, J. B. Chen, Q. X. Ke, J. R. Chang, W. F. Chang, and Y. T. King, "A circular CPW-fed slot antenna for broadband circularly polarized radiation," *Microw. Opt. Technol. Lett.*, vol. 49, no. 11, pp. 2728–2733, Nov. 2007.

[13] T. G. Ma and S. J. Wu, "Ultrawideband band-notched folded strip monopole antenna," *IEEE Trans. Antennas Propag.*, vol. 55, no. 9, pp. 2473–2479, Sep. 2007.

[14] M. J. Ammann and Z. N. Chen, "A wide-band shorted planar monopole with bevel," *IEEE Trans. Antennas Propag.*, vol. 51, no. 4, pp. 901–903, Apr. 2003.

Christina F. Jou was born in Taipei, Taiwan, R.O.C., in 1957. She received the B.S., M.S., and Ph.D. degrees in electrical engineering from the University of California, Los Angeles, in 1980, 1982, and 1987, respectively. The subject of her doctoral thesis was the millimeter wave monolithic Schottky diode-grid frequency doubler.

From 1987 to 1990, she was with Hughes Aircraft Company, Torrance, CA, as a Member of the Technical Staff in the Microwave Products Division, where she was responsible for microwave device modeling. In 1990, she joined National Chiao-Tung University, Hsinchu, Taiwan, where she is now an Associate Professor of communication engineering. Her current research is in developing RF and microwave active circuits and MEMS antennas, and filters.

Jin-Wei Wu was born in Tainan, Taiwan, R.O.C., in 1982. He received the B.S. and M.S. degrees in electrical engineering from Feng-Chia University, Taichung, Taiwan, in 2004 and 2006, respectively.

He is currently working toward the Ph.D. degree in communication engineering at the National Chiao-Tung University, Hsinchu, Taiwan. His research interests include design of microstrip filters and antennas.

Chien-Jen Wang (M'00–SM'05) was born in Kaohsiung, Taiwan, in 1971. He received the B.S. degree in electrical engineering from the National Sun-Yet-Sen University, Kaohsiung, in 1993 and the Ph.D. degree from the National Chiao-Tung University, Hsinchu, Taiwan, in 2000.

In 2000, he joined the Wireless Communication BU, BenQ Corporation, Taipei, Taiwan, as a Project Researcher, where he developed built-in antennas for handsets. In 2001, he joined the Department of Electrical Engineering, Feng-Chia University, Taichung, Taiwan, as an Assistant Professor and an Associate Professor in 2004. Since 2006, he has been with the Department of Electronics Engineering, National University of Tainan, Taiwan, as an Associate Professor. His research activities involve the design and applications of RF/microwave circuits, microstrip antennas, and antenna arrays.